

On the assimilation of optical reflectances and snow depth observations into a detailed snowpack model

Luc Charrois, Emmanuel Cosme, Marie Dumont, Matthieu Lafaysse, Samuel Morin, Quentin Libois, Ghislain Picard

▶ **To cite this version:**

Luc Charrois, Emmanuel Cosme, Marie Dumont, Matthieu Lafaysse, Samuel Morin, et al.. On the assimilation of optical reflectances and snow depth observations into a detailed snowpack model. The Cryosphere, 2016, 10, pp.1021 - 1038. 10.5194/tc-10-1021-2016-supplement . insu-01388769

HAL Id: insu-01388769
https://insu.hal.science/insu-01388769

Submitted on 27 Oct 2016

HAL is a multi-disciplinary open access archive for the deposit and dissemination of scientific research documents, whether they are published or not. The documents may come from teaching and research institutions in France or abroad, or from public or private research centers.

L'archive ouverte pluridisciplinaire **HAL**, est destinée au dépôt et à la diffusion de documents scientifiques de niveau recherche, publiés ou non, émanant des établissements d'enseignement et de recherche français ou étrangers, des laboratoires publics ou privés.

The Cryosphere, 10, 1021–1038, 2016
www.the-cryosphere.net/10/1021/2016/
doi:10.5194/tc-10-1021-2016
© Author(s) 2016. CC Attribution 3.0 License.



The Cryosphere Open Access EGU

On the assimilation of optical reflectances and snow depth observations into a detailed snowpack model

Luc Charrois[1,2], Emmanuel Cosme[1], Marie Dumont[2], Matthieu Lafaysse[2], Samuel Morin[2], Quentin Libois[1], and Ghislain Picard[1]

[1]Université Grenoble Alpes-CNRS, LGGE, UMR 5183, Grenoble, France
[2]Météo-France/CNRS, CNRM UMR 3589, CEN, Grenoble, France

Correspondence to: Luc Charrois (luc.charrois@meteo.fr)

Received: 20 October 2015 – Published in The Cryosphere Discuss.: 14 December 2015
Revised: 7 April 2016 – Accepted: 25 April 2016 – Published: 13 May 2016

Abstract. This paper examines the ability of optical reflectance data assimilation to improve snow depth and snow water equivalent simulations from a chain of models with the SAFRAN meteorological model driving the detailed multilayer snowpack model Crocus now including a two-stream radiative transfer model for snow, TARTES. The direct use of reflectance data, allowed by TARTES, instead of higher level snow products, mitigates uncertainties due to commonly used retrieval algorithms.

Data assimilation is performed with an ensemble-based method, the Sequential Importance Resampling Particle filter, to represent simulation uncertainties. In snowpack modeling, uncertainties of simulations are primarily assigned to meteorological forcings. Here, a method of stochastic perturbation based on an autoregressive model is implemented to explicitly simulate the consequences of these uncertainties on the snowpack estimates.

Through twin experiments, the assimilation of synthetic spectral reflectances matching the MODerate resolution Imaging Spectroradiometer (MODIS) spectral bands is examined over five seasons at the Col du Lautaret, located in the French Alps. Overall, the assimilation of MODIS-like data reduces by 45 % the root mean square errors (RMSE) on snow depth and snow water equivalent. At this study site, the lack of MODIS data on cloudy days does not affect the assimilation performance significantly. The combined assimilation of MODIS-like reflectances and a few snow depth measurements throughout the 2010/2011 season further reduces RMSEs by roughly 70 %. This work suggests that the assimilation of optical reflectances has the potential to become an essential component of spatialized snowpack simulation and forecast systems. The assimilation of real MODIS data will be investigated in future works.

1 Introduction

Seasonal snowpack modeling is a crucial issue for a large range of applications, including the forecast of natural hazards such as avalanches or floods, or the study of climate change (e.g., Durand et al., 1999; Lehning et al., 2006; Bavay et al., 2013). The most sophisticated detailed snowpack models represent the evolution of snow microstructure and the layering of snow physical properties (Brun et al., 1989, 1992; Jordan, 1991; Bartelt and Lehning, 2002; Vionnet et al., 2012) in response to meteorological conditions. Despite constant efforts to improve these models, large uncertainties remain in the representation of the snow physics, as well as in the meteorological forcings (Carpenter and Georgakakos, 2004; Essery et al., 2013; Raleigh et al., 2015). These uncertainties are highly amplified when propagated to avalanche hazard models (Vernay et al., 2015). For operational applications, the assimilation of observations can help reduce the impact of the model and forcing uncertainties in the snowpack simulations (e.g., Dechant and Moradkhani, 2011).

Satellite observations are becoming an essential component of snow modeling and forecasting systems. In situ measurements are the most detailed and accurate observations of the snowpack, but their spatial distribution is far too scarce to capture the high spatial variability of the seasonal snowpack properties and improve snowpack simulations through

their assimilation. For this reason, the assimilation of satellite observations of snow is an active area of research.

Snow remote sensing is primarily performed in the microwave (passive and active), visible and near-infrared spectra. Since the direct assimilation of such data requires the use of radiative transfer models, a common and simple approach consists in using satellite-based snow products. In particular, the assimilation of snow cover fraction (SCF) estimates derived from optical sensors (such as MODIS) and snow water equivalent (SWE) or snow depth (SD) estimates derived from passive microwave sensors (such as AMSR-E) has been investigated extensively (Sun et al., 2004; Andreadis and Lettenmaier, 2006; Clark et al., 2006; Dong et al., 2007; De Lannoy et al., 2012; Liu et al., 2013).

These studies have suggested that, most of the time, assimilating snow observations may be useful to improve snowpack estimation. SWE or SD assimilation generally outperforms the assimilation of SCF only, except from Andreadis and Lettenmaier (2006) because of large errors in the AMSR-E SWE products. The assimilation of both combined revealed larger benefit by mitigating sensors limitations. Recently, Navari et al. (2016) investigated the assimilation of (synthetic) ice surface temperature while Dumont et al. (2012) also experimented the assimilation of albedo retrievals, both from optical sensors. Dumont et al. (2012) obtained a mass balance RMSE decrease of up to 40 % assimilating albedo data. However, satellite snow products are derived using retrieval algorithms which are not perfect and, perhaps more importantly, not physically consistent with the snowpack model used for the data assimilation. For this reason, and as advocated by Durand et al. (2009) who tested the assimilation of in situ microwave radiance observations, assimilating the original satellite radiance data should be preferred when possible.

The potential of assimilating passive microwave radiances (in the form of brightness temperature) collected by AMSR-E satellite have been examined by Dechant and Moradkhani (2011) and Che et al. (2014). Significant improvements in the SWE/SD predictions occurred but only during the accumulation period. Though the melt period, when the snowpack is wet, liquid water alters the microwave signal resulting in a lower performance of the assimilation. Moreover, for small-scale applications in mountainous areas, the coarse spatial resolution of these data considerably reduces their usefulness (Foster et al., 2005; Cordisco et al., 2006; Dong et al., 2007; Tedesco et al., 2010). As for active microwave measurements, several tests have been conducted to assimilate the satellite signal (e.g., Stankov et al., 2008; Phan et al., 2014). These tests were however limited by the accuracy of the forward electromagnetic models and by the current lack of satellite data at a daily or even weekly time frequency.

Visible and near-infrared reflectances from satellite observations have never been assimilated into snowpack models despite their great sensitivity to the snowpack properties (Warren, 1982). Even if cloud cover might limit their utility, medium and high spatial resolution data are available at daily resolution from several optical sensors (e.g., MODerate resolution Imaging Spectrometer, Visible Infrared Imaging Radiometer Suite) and seem to be quite suitable for complex topography (Sirguey et al., 2009). In particular, the MODIS sensor, onboard the TERRA and AQUA satellites, offers a daily coverage and provides reflectance measurements in seven bands distributed in the visible (at 250 to 500 m spatial resolution), near and shortwave infrared wavelengths. Surface bi-hemispherical reflectances corrected from complex topographic effects in mountainous areas can be computed (Sirguey et al., 2009) and have been evaluated and used in several rugged areas (Dumont et al., 2012; Brun et al., 2015).

The work presented in this article examines the possibility, the relevance and the limitations of assimilating visible and near-infrared satellite reflectances into a multilayer snowpack model. A convenient approach, known as twin experiment, uses synthetic data in the same spectral bands than the real data, to examine the content of information of the observations, and the impacts we can expect from their assimilation. In twin experiments, the model used to create the synthetic data is the same as the model used for the assimilation. The synthetic observations are extracted from a member of the ensemble considered as the true state. Twin experiments are preferred in this first study in order to focus on the information content of the observations and to avoid the problem of observational biases. Data assimilation is performed with a particle filter and a Sequential Importance Resampling (SIR) algorithm (Gordon et al., 1993; Van Leeuwen, 2009, 2014). The particle filter is easy to implement, free of hypotheses about the nature of the model and the observations, and provides uncertainties in the estimation of the snowpack state.

For a comprehensive snow simulation evaluation, as recommended by Essery et al. (2013), our study is based on five hydrological seasons (2005/2006, 2006/2007, 2009/2010, 2010/2011, 2011/2012) which represent a wide range of possible snow cover conditions in the Alpine area. Moreover, two experimental sites were used in this work in virtue of a long, continuous time series of meteorological data and an area suitable for remote sensing measurements. The Col de Porte (CdP) area, located in the Chartreuse area, near Grenoble, France (1325 m a.s.l.) provides a data set from 1993 to present (Morin et al., 2012) from which meteorological statistics can be estimated, but the instrumentation and surrounding forest at this site may affect satellite measurements. For this reason, assimilation experiments are carried out at the Col du Lautaret (CdL) located (2058 m a.s.l.) in the Ecrins area, France, which exhibits a large flat open area, above treeline, more suitable for remote sensing. Consequently, an ensemble of perturbed forcing was generated in order to represent the range of possible weather conditions at the CdL area. To this end, we developed a stochastic

method using a first-order autoregressive model based on the estimated meteorological uncertainty.

In Sect. 2, the SURFEX/ISBA – Crocus snowpack model used in this study is described with an emphasis on the characteristics that affect the implementation of the data assimilation method. In particular, we consider the meteorological forcings as the only source of uncertainties. Section 3 presents in detail how these forcings are perturbed to take the uncertainties into account in the design of the ensemble simulations. The experimental setup and the data assimilation implementation are presented in Sect. 4. The results of the reference assimilation experiment (baseline experiment) using synthetic reflectance observations at one point are presented and discussed in Sect. 5. In close relation to this baseline experiment, results of different sensitivity tests are addressed in Sect. 6.

2 SURFEX/ISBA – Crocus

2.1 A brief overview

The unidimensional detailed multilayer snowpack model Crocus (Brun et al., 1989, 1992) simulates the evolution of the snowpack physical and microstructural properties driven by near-surface meteorology and includes a representation of snow metamorphism. A detailed description of Crocus is provided by Vionnet et al. (2012); here we only emphasize aspects that are key to data assimilation. The snowpack is vertically discretized into snow layers with different physical properties and a dynamic layering scheme handles its evolution (see details in Sect. 2.2). The evolution of the snow cover is a function of energy and mass transfer between the snowpack, the atmosphere and the ground. The model simulates the major physical processes of snowpack evolution such as heat conduction, light penetration, water percolation and refreezing, settlement and snow metamorphism.

Crocus has been run operationally at Météo-France in support of avalanche risk forecasting over the last 20 years (Durand et al., 1999). It has been also successfully used for various applications such as climate studies or hydrology (e.g., Etchevers et al., 2001; Castebrunet et al., 2014). Recently, Crocus has been integrated into the SURFEX externalized surface modeling system (Masson et al., 2013) as one of the snow schemes within the Interactions between Soil, Biosphere and Atmosphere (ISBA) land surface model (Noilhan and Planton, 1989). Thus the integrated system simulates the energy fluxes between the snow cover and the multilayer soil component of the land surface model (ISBA-DIF, Boone and Etchevers, 2001).

2.2 Layering

In Crocus, the snowpack is vertically discretized in order to realistically simulate the time evolution of a stratified snowpack. The layering scheme is dynamic in order to preserve snowpack history and maintain the possible thin and weak snow layers within the snowpack. The number of layers ranges from 0 (bare soil) to a maximum of 50, typically. Layering is updated at the beginning of each time step. It consists in adding, removing, or merging layers depending on their physical properties and thicknesses. The procedure basically follows this set of rules:

- For a snowfall on an existing snowpack, fresh snow is incorporated into the top layer if (i) snow microstructure characteristics are similar, (ii) the top layer is thinner than 1 cm and (iii) the snowfall intensity is inferior to $0.03\,\mathrm{kg\,m^{-2}\,h^{-1}}$. If one of these criteria is not met or change during the time step, a new top layer is created.

- A snowfall on bare soil forms a snowpack with a set of identical layers, the number of which depends on the quantity of fallen snow.

- In absence of snowfall, the model first seeks to merge two thin and adjacent layers with similar microstructure characteristics, or inversely, split the thick ones. When the number of layers has reached a maximum of 50, layers that are too small relative to a prescribed optimal vertical profile are aggregated with adjacent ones. This idealized thickness profile depends on the current snow depth and on the user-defined maximal number of layers. To reach the optimal vertical profile, the model first seeks to thin the top layers, most subject to the exchange of energy, and then to keep an appropriate thickness ratio between adjacent snow layers to prevent numerical instabilities in the resolution of the heat diffusion equation through the snowpack.

- Most of the time, compaction makes layers thinner without grid resizing.

Dynamic layering adds an extra challenge in the assimilation of observations with Crocus. Data assimilation methods commonly used in geophysics are well designed for fixed-grid models. For example, the Ensemble Kalman filter involves the averaging of different snow profiles. This specificity of Crocus largely determines our data assimilation method, as it will be discussed in Sect. 4.3.

2.3 Penetration of solar light in the snowpack

Given that satellite observations indirectly relate to the quantities of interest, an observation operator is required to link the satellite observation and the model state variables (Reichle, 2008). This operator transforms the model variables into diagnostic variables to allow a direct comparison with satellite observations, preserving the physical consistency of the satellite signal with the snow model.

To this end, a new radiative transfer model was recently implemented in Crocus to calculate spectral reflectances that can be used for the comparison and the assimilation

of satellite observations data such as MODIS data. This model, named TARTES (Two-streAm Radiative TransfEr in Snow, Libois et al., 2013, 2014), simulates the absorption of solar radiation within the stratified snowpack using the δ-Eddington approximation, with a spectral resolution of 20nm. This contrasts with the original version of Crocus, where albedo was computed for three large spectral bands only and from the properties of the first two layers (Brun et al., 1992; Vionnet et al., 2012).

TARTES is implemented as an optional module to be called instead of the original Crocus albedo scheme. This implementation has no significant impact on the model structure but increases the computation time of roughly a factor 10 depending on the number of snow layers and the snow depth. TARTES makes use of four Crocus prognostic variables (specific surface area – SSA, density, snow layer thickness, impurity content) and the angular and spectral characteristics of the incident radiance (e.g., the solar zenith angle and the presence of cloud cover). The computation of SSA has recently been implemented by Carmagnola et al. (2014).

The use of a full radiative transfer model embedded within the snowpack model enables the assimilation of the satellite reflectance data, therefore avoiding the introduction of uncertainties from an external retrieval algorithm. And beyond its use for the assimilation of reflectances, TARTES also provides a more accurate calculation of light absorption parameters, leading to better simulations of the snowpack.

2.4 Snow impurities

Snow surface reflectance in the visible spectrum depends on the content of light-absorbing impurities in the snowpack (Warren, 1982). The impurity content can have a major impact on the snowpack simulations (Dumont et al., 2014). Despite efforts to improve the knowledge and the modeling of impurities in snow (e.g., Warren and Clarke, 1990; Domine et al., 2004; Painter et al., 2007; Doherty et al., 2013), snow impurity deposition and evolution remain poorly quantified.

Currently implemented in a version of SURFEX/ISBA – Crocus, the radiative model TARTES (introduced in Sect. 2.3) calculates the impurity content as an equivalent black carbon content (Doherty et al., 2013; Gabbi et al., 2015). This impurity content evolves according to (i) the impurity content in fresh snow, c_0, (ii) the time of exposure of the layer at the surface and (iii) the dry deposition flux of impurity, τ_{dry} as described in the equation below.

$$c(t+\Delta t) = c(t) + \Delta t\, \tau_{\mathrm{dry}} e^{-D/h_{\mathrm{ref}}}, \quad (1)$$

where $c(t)$ is the impurity content at time t, D is the depth of the middle of the considered snow layer and $h_{\mathrm{ref}} = 5\,\mathrm{cm}$ is the e-folding of the exponential decay rate for the deposition of snow impurities ensuring that only the top layers are influenced by dry deposition.

2.5 Atmospheric forcings

The snowpack evolution strongly depends on near-surface meteorological forcings. These forcings are provided by the meteorological downscaling and analysis tool SAFRAN (Système d' Analyse Fournissant des Renseignements Atmosphériques à la Neige; Durand et al., 1993). SAFRAN is used to drive snowpack simulations in the French mountains because it is designed to operate at the geographical scale of meteorologically homogeneous mountain ranges, varying from 400 to 2000 km^2. The model combines vertical profile estimates from the ERA-40 re-analysis with observed weather data from the automatic surface observations network at different elevations, the French Snow/Weather network, rain radars, and rain gauges. As outputs, SAFRAN provides meteorological data to the snowpack model with an hourly time step for all slopes and aspects, and a 300 m-elevation step.

3 Design of Crocus ensemble simulations

3.1 General strategy

In view of assimilating observations to reduce snowpack simulation uncertainties, we first need to represent them. As shown in Raleigh et al. (2015), the meteorological forcings are the major source of uncertainty in snowpack simulations (when a meteorological model is used to drive the snow model). In the present study, air temperature, wind speed, snowfall and rainfall rates, shortwave and longwave radiative fluxes, and the deposition rate of impurities will thus be considered as the only sources of uncertainty. Snowpack model errors introduced by metamorphism and other parameterizations of physical laws are not taken into account here. The characterization and representation of these errors, notably in the perspective of real data assimilation, will be addressed in a future and dedicated work. An identified option is to use multi-physics ensemble simulations.

We implement an ensemble method to represent the uncertainties in the forcings and their impact on snowpack simulations. An ensemble of possible realizations of the atmospheric forcings is formed and used to compute an ensemble of snow profiles representing the probability distribution of the model simulation. The following section describes the construction of the ensemble of meteorological forcings and the response of the model to this source of uncertainty, without assimilation.

3.2 Quantification of meteorological forcing uncertainties

To quantify and calibrate the meteorological forcing uncertainties, we compare 18 years of surface meteorology from SAFRAN reanalysis with in situ observations at the CdP site. A long time-series from 1993 to present (Morin et al., 2012)

being available at this site, uncertainties in the SAFRAN meteorological reanalysis can be estimated.

Table 1 (left column) reports the bias and the standard deviation (STD) of the difference between SAFRAN and the observations carried out at the CdP site, for each meteorological variable (values in brackets and the right column report other data discussed later). The table reflects differences between SAFRAN and in situ observations, resulting, from the different spatial representativities of both sources, the intrinsic errors of the analysis system and measurement errors.

As highlighted by Quintana Segui et al. (2008) who conducted an extended evaluation of SAFRAN reanalysis but over a shorter period (one year), the large discrepancies between the model and the observations can be explained by local effects due to orography and vegetation and, for the precipitation and wind speed, by the time interpolation necessary to obtain hourly forcing fields from the daily analysis. For example, the precipitation analysis is performed on a daily basis in order to include in the analysis the numerous rain gauges observations. Radiation fluxes uncertainty might be attributed to biases in cloud coverage and altitude estimates, effects of vegetation and surrounding slopes that are not taken into account for longwave estimates. Finally, the shading mask for shortwave radiation does not account for vegetation evolution that can also lead to shortwave flux discrepancies. Durand et al. (2009) carried out, only on a limited set of variables, a more systematic evaluation of SAFRAN for the 1958–2002 period using 43 sites in the French Alps. Averaged over all locations, the RMSE on air temperature are similar to the one computed in our study. However, their results also highlight the spatial variability of SAFRAN performance (site RMSE ranges from -0.8 to $+1.5\,^{\circ}\mathrm{C}$). Nevertheless, this will not have a strong impact in this study since it is based on twin experiments.

3.3 Building the ensemble of meteorological forcings

The sample of meteorological forcings is formed by perturbing the original SAFRAN reanalysis with a random noise commensurate with the actual uncertainty. We thus build an ensemble of meteorological forcings with a negligible bias with respect to the SAFRAN reanalysis and a standard deviation close to the one computed from CdP statistics (Table 1, left column).

To keep the procedure simple and preserve physically consistent time variations of the forcings, the random perturbations are computed using a first-order autoregressive – AR(1) – model (Deodatis and Shinozuka, 1988) for each variable:

$$X_{\mathrm{t}} = \varphi X_{\mathrm{t\text{-}1}} + \epsilon_{\mathrm{t}}, \tag{2}$$

with X being the perturbation value at time t and $t-1$. φ is the AR(1) model parameter and can be written $\varphi = e^{\frac{-\Delta t}{\tau}}$, Δt being the time step and τ the decorrelation time. Parameter τ is adjusted for each variable, so that the perturbed variable exhibits the same frequency of temporal variations than the original variable (Fig. S1 bottom, in the Supplement, in blue).

The amplitudes of the meteorological uncertainties are introduced with ϵ_{t}, a white noise process with zero mean and constant variance σ^2. Variance σ^2 is computed from each standard deviation of the residuals between the reanalysis and observations at CdP (σ_{CdP}: Table 1, left column) following this equation:

$$\sigma^2 = \sigma_{\mathrm{CdP}} \times (1-\varphi^2). \tag{3}$$

Finally, for each meteorological variable, the selection of an additive or multiplicative perturbation method is driven by (i) the nature of the variable (ii) the dependency of the model–measurement difference to the measured values as detailed below.

For precipitation rates, shortwave radiation and wind speed, the choice of a multiplicative method is motivated by the following reasons:

- SAFRAN reanalysis effectively captures the occurrence of precipitation (since it assimilates surface observation network) but are more subject to errors in the amount of precipitation;
- Regarding shortwave flux and wind speed, the model biases exhibit a linear dependency to the value of the variable (not shown). Consequently, a multiplicative method was selected.

For longwave radiation and air temperature, given that there is no dependency between the model biases and the field values, an addition method is chosen.

At every time step the perturbation X_{t} is applied as follows.

For the additive method, $\mathrm{variable}_{\mathrm{t}} = \mathrm{variable}_{\mathrm{t}} + X_{\mathrm{t}}$. For the multiplicative method, the perturbation is centered on 1 (Y_{t}) before multiplying the variable.

$$Y_{\mathrm{t}} = X_{\mathrm{t}} + 1$$

$$\mathrm{variable}_{\mathrm{t}} = \mathrm{variable}_{\mathrm{t}} \times Y_{\mathrm{t}}.$$

For the multiplicative method, the perturbations are bounded by 0.5 and 1.5 to avoid extreme values. The result from this perturbation method is illustrated by Fig. S1 which shows the SAFRAN snowfall rates over a 1-week period, a realization of the perturbed analysis and the full ensemble of perturbed analysis.

To maintain further physical consistency between the meteorological variables, snowfall is changed to rainfall if air temperature is higher than $274.5\,^{\circ}\mathrm{K}$ and the shortwave radiation is bounded to $200\,\mathrm{W\,m^{-2}}$ in case of rain or snow fall due to the inherent cloud cover. This behavior is consistent with the CdP statistics where over 18 years, during a precipitation period, the measured in situ shortwave radiation rarely exceeds $200\,\mathrm{W\,m^{-2}}$.

Table 1. Bias and standard deviations (STDs) of the differences between SAFRAN reanalysis and in situ observations (left) and the differences between SAFRAN reanalysis and the ensemble built up in the present study (right), for the perturbed meteorological forcings. The first set of statistics is derived from 18 years (1993–2011) of observations and reanalysis at the CdP and the second set is derived from our 300-members ensemble over the 2010/2011 hydrological season. The values in brackets correspond to the adjusted standard deviation used to generate the ensemble at CdL site.

	CdP: Reanalysis – Observations		CdL: Reanalysis – Ensemble	
Variables	Bias	STD: σ_{CdP}	Bias	STD: σ_{CdL}
Air temperature (C)	0.28	1.08	5.0×10^{-3}	1.07
Wind speed ($\mathrm{m\,s^{-1}}$)	0.2	1.12 (0.6)	4.0×10^{-4}	0.4
Shortwave radiation ($\mathrm{W\,m^{-2}}$)	22.4	79 (70)	-3.1×10^{-3}	58.3
Longwave radiation ($\mathrm{W\,m^{-2}}$)	−14.0	24.5 (7)	2.0×10^{-2}	7.0
Snowfall rate ($\mathrm{kg\,m^{-2}\,h^{-1}}$)	-2.0×10^{-2}	0.4	5.0×10^{-3}	0.1
Rainfall rate ($\mathrm{kg\,m^{-2}\,h^{-1}}$)	7.2×10^{-3}	0.5	-5.0×10^{-3}	0.1

Ensembles are generated with model errors coming from the statistics of the CdP site but as explained previously, the assimilation framework is based on the CdL area. Some adjustments in the building of ensembles are also required to account differences between these two areas.

In particular, the forest at CdP affects the local wind field and the radiative fluxes (Morin et al., 2012), which explains a large part of the variability of SAFRAN errors at CdP. At CdL, an open meadow area, such variability is unlikely. To limit the overspreading of the forcing ensemble, the standard deviation used in the Eq. (3) for wind speed, short and longwave radiation are reduced to $0.6\,\mathrm{m\,s^{-2}}$, 70 and $7\,\mathrm{W\,m^{-2}}$, respectively, against $1.12\,\mathrm{m\,s^{-2}}$, 79 and $24.5\,\mathrm{W\,m^{-2}}$ (Table 1, left column, values in brackets). As shown in Table 1, the standard deviations computed from the generated ensemble (right column) are close to the ones prescribed to generate it (left column).

In the end, this stochastic method of perturbations makes possible the construction of an ensemble of perturbed forcings which are required when using ensemble methods. The calibration of the perturbations are based on the CdP statistics while their temporal correlation is ensured by the AR(1) model. The perturbation method exhibits some obvious limitations. Inter-variable correlations are indeed not taken into account in the ensemble except from the precipitation phase and the maximum value of shortwave radiation in case of precipitation. Adjustments to CdL are somewhat subjective, but this is not crucial in our twin experiment context since the considered truth will be simulated running Crocus with one forcing member drawn from this generated ensemble. A more physically consistent ensemble will be required when real data assimilation is investigated.

3.4 Perturbation of impurity deposition rate

In this study, the deposition fluxes of impurities are also considered as a meteorological forcing but unlike meteorological variables previously mentioned (Sect. 2.5), the deposition fluxes of impurities are not provided by the SAFRAN model. Instead, the impurity content in fresh snow c_0 and the dry deposition flux τ_{dry} are perturbed online during a model run.

The parameters c_0 and τ_{dry} are subject to multiplicative perturbations drawn from lognormal distributions. The perturbations are constant in time, but are reinitialized at each observational update when data assimilation is performed. For c_0, the probability density function (pdf) parameters are $\sigma = 0.8$ and $\mu = 0$. c_0 is bounded at 0 and $500\,\mathrm{ng\,g^{-1}}$ and the mode value of the pdf is $100\,\mathrm{ng\,g^{-1}}$. As for τ_{dry}, the pdf parameters are $\sigma = 1.2$ and $\mu = 0$. τ_{dry} is bounded at 0 and $0.5\,\mathrm{ng\,g^{-1}\,s^{-1}}$ with a mode value of $0.015\,\mathrm{ng\,g^{-1}\,s^{-1}}$. These values have been selected to obtain the same order of magnitude of albedo decrease with snow age as in the original Crocus formulation (Brun et al., 1992).

3.5 Ensemble simulations

To investigate the impact of the stochastic perturbations, an ensemble of 300 simulations of the snowpack, forced by the 300 forcings of the meteorological ensemble, is run over the 2010/2011 hydrological season without data assimilation. Figure 1 presents the result of the ensemble simulation with 300 members (represented by the black lines). The simulation forced by the unperturbed reanalysis (red line) is included within the envelope of the ensemble. The spread of the ensemble reflects the consequences of possible overestimations and underestimations of meteorological data by the reanalysis.

The spread of the SD and SWE ensembles (Fig. 1b–c) is the largest at the end of the season, leading to a range of 24 days from the first to the last member to fully melt. The maximum dispersion range of SWE ($\Delta\mathrm{SWE} \approx 300\,\mathrm{kg\,m^{-2}}$) occurs in early April. At this time, the snowpack in some ensemble members has just started to melt, while in other cases, the snowpack has already disappeared.

Snowfalls reset all members to high reflectance values (at 640 nm, 0.98 for a significant event, Fig. 1a) and drastically

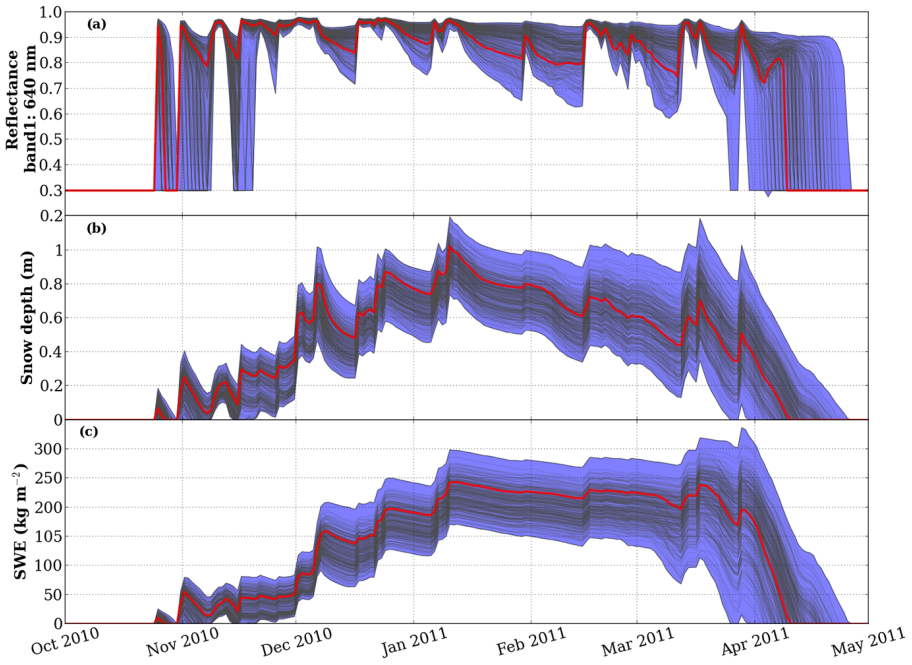


Figure 1. Ensemble simulation with 300 members at the Col du Lautaret site over the 2010/2011 hydrological season. **(a)** – reflectance at 640 nm (center of band 1 of MODIS), **(b)** SD, and **(c)** SWE. On each graph, the red solid line is the simulation forced by the unperturbed SAFRAN analysis. The blue patterns represent the envelopes including the 300 members which are shown by the black lines.

reduce the spread of the reflectance ensemble. Concomitantly, the SD and SWE ensemble spreads can increase due to the uncertainties in the precipitation rates. After a snowfall, impurity content and grain size increase along with the age of snow, decreasing the surface reflectance. This evolution is also influenced by atmospheric forcings, which are slightly different from one ensemble member to another, enlarging the spread of the ensemble. We can therefore expect that the timing of the available reflectances will strongly affect the impact of their assimilation on the snowpack ensemble simulations.

3.6 Dispersion of the ensemble of Crocus simulations

Here we assess whether our ensemble represents a realistic spread of SD over time with respect to previous evaluations of the model through a spread-skill plot.

Given that no SD measurements were systematically carried out at the CdL site, we were not able to evaluate our ensemble spread from SAFRAN-Crocus simulations with a time series of in situ measurements at this site. But, as demonstrated by Fortin et al. (2014), the ability of the ensemble spread to depict the simulation error can be evaluated by the comparison of the RMSE and the ensemble spread (Spd) with respect to the ensemble mean.

Firstly, using the method previously described, an ensemble of Crocus simulations was carried out at the CdP site, with no adjustment on CdP statistics, to evaluate the relevance of our perturbation method by comparing the RMSE between SAFRAN-Crocus simulation and in situ measurements with the Spd of the CdP ensemble. Then, we compare the Spd of our ensemble simulation at the CdL site with a SAFRAN-Crocus RMSE computed from the difference between SD Crocus estimates with in situ SD measurements across multiple stations (at the same elevation than CdL). We used roughly 60 daily snow depth measurements stations from the Météo-France observation stations network (only stations within the same altitude range as the CdL site (1800–2200 m a.s.l.).

The multiple station RMSE and Spd terms are defined as follows, for a variable X,

$$\mathrm{Spd}(X) = \left(\frac{1}{M} \sum_{\mathrm{t}=1}^{M} \frac{1}{N_\mathrm{e}} \sum_{n=1}^{N_\mathrm{e}} \left(X_{\mathrm{t},\,n} - \bar{X}_\mathrm{t} \right)^2 \right)^{1/2}, \quad (4)$$

$$\mathrm{RMSE}(X) = \left(\frac{1}{M} \sum_{\mathrm{t}=1}^{M} \frac{1}{N_k} \sum_{k=1}^{N_k} \left(X_{\mathrm{t},\,k}^{\mathrm{model}} - X_{\mathrm{t},\,k}^{\mathrm{in\,situ}} \right)^2 \right)^{1/2}, \quad (5)$$

where M represents the number of time steps, N_e the size of the ensemble and N_k the number of in situ measurements. The SD value of the ensemble member n at the date t is $X_{\mathrm{t},\,n}$ and $\bar{X}_\mathrm{t}$ is the mean of the ensemble at the date t. The value from SAFRAN-Crocus simulation at the measurement site k and at the date t is given by $X_{\mathrm{t},\,k}^{\mathrm{model}}$, and $X_{\mathrm{t},\,k}^{\mathrm{in\,situ}}$ is the value from the in situ SD measurement. RMSE and Spd are computed at observation times. For comparisons based on only

one point, the RMSE equation for a variable X becomes

$$\mathrm{RMSE}(X) = \left(\frac{1}{M} \sum_{\mathrm{t}=1}^{M} \left(X_{\mathrm{t}}^{\mathrm{model}} - X_{\mathrm{t}}^{\mathrm{in\ situ}} \right)^2 \right)^{1/2}. \quad (6)$$

Figure 2a shows that at the CdP site the SD dispersion (Spd) of the ensemble is consistent with the RMSE between SAFRAN-Crocus simulation with respect to in situ measurements at this site. This suggests that our perturbation method is able to represent the forcing uncertainties on snowpack simulations. Nevertheless, concerning the CdL area over the 2010/2011 season, the SAFRAN-Crocus RMSE is roughly 2 times higher than the SD dispersion (Spd) of our ensemble (Fig. 2b). This means that our ensemble is under-dispersive in terms of SD. This may be partly explained by the calibration of perturbations, based on statistics at a location (CdP) which is not highly affected by wind erosion/accumulation in contrast to many other measurement sites. In addition, only meteorological errors are considered in our ensemble, whereas the other model errors also contribute to the simulation error.

Nonetheless, given that experiments in the present work are twin and that the observations are selected within the ensemble (synthetic observations), the impact of this under dispersion is not crucial, but will be considered when using real data.

4 Data assimilation setup

This section describes the assimilation framework and the assimilation strategies designed for this study prior to presenting results of assimilation experiments (Sect. 5 and 6). First of all, the experimental setup and diagnostics applied in this study are detailed before describing the two synthetic observational data sets used for assimilation. An overview of the SIR filter is given at the end of this section and further details are provided in the Appendix A.

4.1 General settings and diagnostics

The assimilation experiments are twin, meaning that the observations are synthetics and come from a single model simulation. They are performed over five winter seasons at the CdL area.

A synthetic truth simulation is first obtained by running Crocus, through the use of the radiative transfer model TARTES, forced by one perturbed meteorological forcing, as detailed in Sect. 3.3. The synthetic observations used in all the assimilation experiments reported in Sects. 5 and 6 are extracted from this synthetic truth simulation. The synthetic truth simulation is also considered as the truth to evaluate the performance of data assimilation in terms of SD and SWE variables.

Data assimilation performances are evaluated by comparing RMSE for ensembles with and without assimilation, and by comparing the synthetic true simulation to the 33rd, 50th, and 67th quantiles from the ensembles with assimilation.

For a variable X, the ensemble RMSE is defined as

$$\mathrm{RMSE}(X) = \left(\frac{1}{N_{\mathrm{e}}} \sum_{n=1}^{N_{\mathrm{e}}} \left(X_n - X^{\mathrm{truth}} \right)^2 \right)^{1/2}, \quad (7)$$

where N_{e} represents the size of the ensemble, X_n the value from the ensemble member n, and X^{truth} the value from the synthetic truth. RMSEs are computed at observation times. The uncertainty on the melt-out date is quantified as the difference (in days) between the first and the latest full melted member.

4.2 Nature of the assimilated observations

The first set of synthetic observations is composed of surface reflectances of the first seven bands of MODIS (central wavelengths: 460, 560, 640, 860, 1240, 1640, 2120 nm; Hall and Riggs, 2007). In twin context, these synthetic observations are provided from the synthetic truth simulation running Crocus with its radiative TARTES model. Snow surface reflectances in the visible and near-infrared spectra are sensitive to the properties of the first millimeters to the first centimeters of the snowpack for a given wavelength (Li et al., 2001). They mainly vary with snow microstructure (near-infrared part) and impurity content (visible part) (Warren, 1982). The reflectance observations error variances, necessary for the assimilation, are defined according to Wright et al. (2014). They are prescribed to 7.1×10^{-4}, 4.6×10^{-4}, 5.6×10^{-4}, 5.6×10^{-4}, 2.0×10^{-3}, 1.5×10^{-3} and 7.8×10^{-4}, for the seven bands, respectively. In the framework of our twin experiments, the covariance matrix of observation errors is diagonal. Note that the TARTES model calculates bi-hemispherical reflectances while the satellite measurements provide directly hemispherical-conical top of atmosphere reflectances (Dumont et al., 2012).

The second set of observations is composed of synthetic snow depth (SD) observations. Previous studies have indeed reported that the assimilation of snowpack bulk variables such as SD greatly improve snow estimations (Morin, 2014; Liu et al., 2013). However, SD observations are only available at one point. In our study, the observation error variance of SD is taken to be 0.003 m (corresponding to a standard deviation of about 5 cm). The impact of synthetic SD assimilation is detailed in Sect. 6.3.

The setup designed in our study (one point, twin experiments) allows relevant comparisons of the benefits of assimilating separately or jointly the two above mentioned types of observations. For future works assimilating real data, the difference in the geometrical configuration between the simulated TARTES reflectances and satellite observations will be addressed.

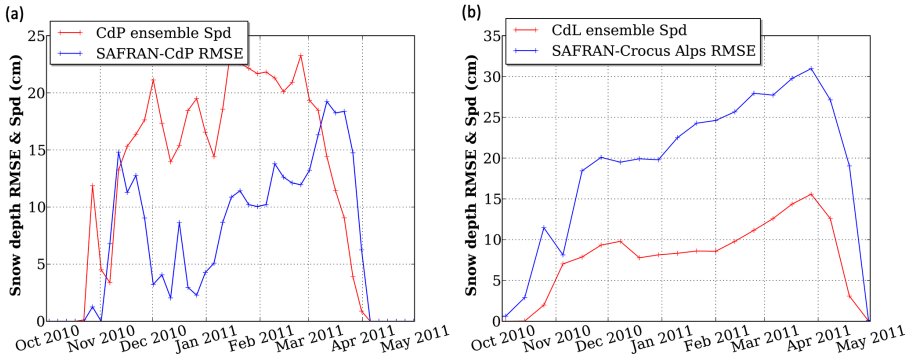


Figure 2. Time evolution over the 2010/2011 season of (in red) the SD ensemble Spd with respect to the ensemble mean and (in blue) the SD RMSE between SAFRAN-Crocus estimates and in situ observations, **(a)** for the CdP site and **(b)** for the CdL ensemble compared to the multiple Alps stations at the same elevation as CdL.

4.3 Assimilation method: the particle filter

The data assimilation method has been chosen after considering the requirements and the possible degrees of freedom that our problem imposes or offers.

Firstly, we require that the method quantifies uncertainties. This plays in favor of ensemble methods (e.g., Blayo et al., 2014). Secondly, we prefer an already existing and well tested method. This argues for the Ensemble Kalman Filter (EnKF, Evensen, 2009) or the particle filter (Van Leeuwen, 2009, 2014). Thirdly, the method should not rely on assumptions about the physical system, such as linearity or weak nonlinearity, because the physics of our model are nonlinear. This draws us toward the particle filter. Fourthly, the method should be easy to implement for this first study. Abaza et al. (2015) assessed the effectiveness assimilating streamflow data using an EnKF sequential procedure but implemented in a simpler snow scheme than Crocus. The fact that the EnKF involves state-averaging operations, to which Crocus hardly complies due to its varying number of snowpack layers, argues in favor of the particle filter. Note that Dechant and Moradkhani (2011) also chose the SIR filter for the assimilation of microwave radiances in a snowpack model. The major drawback of the particle filter is that it is not applicable to high-dimensional systems (Snyder et al., 2008) because it quickly degenerates (all ensemble members converge toward a unique and spurious model trajectory). But our model, with hardly more than a few hundreds of variables, is not high-dimensional. Our experiments show it indeed does not degenerate if a well-tested resampling method is used, with ensembles of a few hundreds of members only. Thus, we choose the sequential importance resampling (SIR) filter (Gordon et al., 1993), which is a particular type of the particle filter. Our ensembles are composed of 300 members.

The SIR filter seeks to represent the probability density function (pdf) of the model state by a discrete set (an ensemble) of states commonly called particles. The propagation over time of all particles, through the nonlinear model equations, describes the evolution of the model pdf. When observations are available, the ensemble is updated following two steps: (i) the particles are weighted according to their respective distances from the observations, and (ii) the pdf defined by the newly weighted particles is resampled by ruling out particles with negligible weights, and duplicating particles with large weights, so that the updated pdf is again represented by an ensemble of equally weighted particles. The new ensemble is then ready to be propagated in time by the model. As long as a particle is not removed, it keeps its original perturbed forcing to be propagated. Inversely, a new perturbed forcing is assigned to a duplicated particle for propagation to the next analysis. The governing equations of the data assimilation scheme are given in the Appendix A and more details are presented in Van Leeuwen (2009, 2014).

5 Assimilation of MODIS-like reflectances

In this section, we assess to what extent the assimilation of the available MODIS-like reflectance observations allows the accurate estimation of snowpack properties throughout the season. This experiment will be considered as our baseline experiment.

Data assimilation results for the 640 and 1240 nm reflectance (first and fifth MODIS bands) and for SD and SWE over the hydrological season 2010/2011 are shown in Fig. 3. To mimic real cloud conditions, reflectances are assimilated at 34 clear sky days of the season. We define a clear sky date according to the real cloud mask from MODIS data computed with the method of Sirguey et al. (2009). The corresponding 640 and 1240 nm synthetic reflectance observations are shown by the red dots in Fig. 3a and b. The control simulation (from which the synthetic observations are drawn) is shown by the red lines.

Throughout the season, the envelopes of SD and SWE ensembles for the baseline experiment (Fig. 3, blue envelopes) include the control simulation, which is a prerequisite for the good behavior of the assimilation. Overall, the assimi-

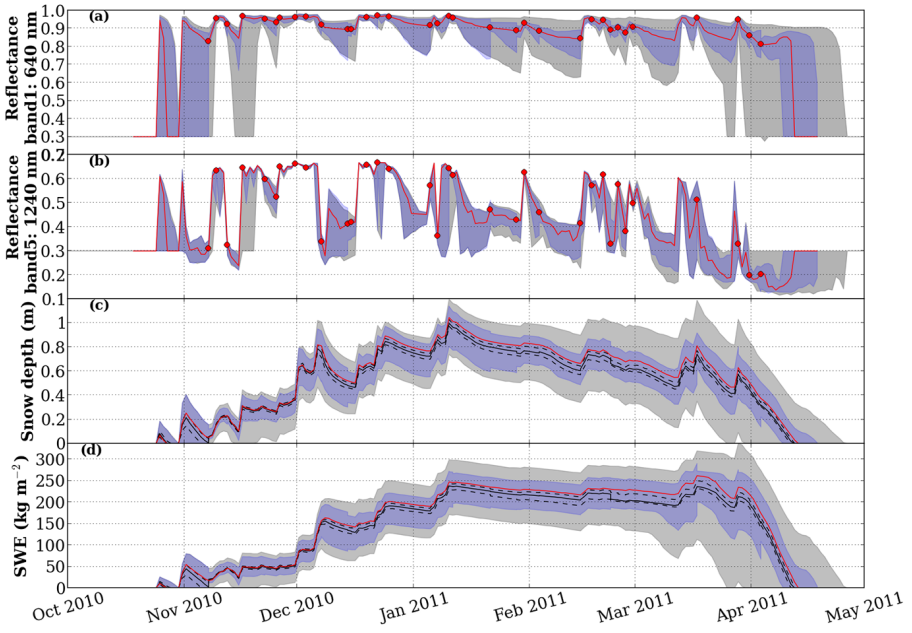


Figure 3. Evolution of the ensemble over the 2010/2011 season, **(a)** and **(b)** – reflectance at 640 and 1240 nm (first and fifth MODIS band, respectively), **(c)** SD and **(d)** SWE. The blue shading represent the envelopes of the ensemble assimilating MODIS-like reflectances and the grey shading the envelopes of the ensemble without assimilation. The red lines represent the control simulation (synthetic truth). In graph **(a)** and **(b)**, the red dots show the assimilated observations. In both **(c)** and **(d)**, the black solid line shows the 50 % quantiles (median of the ensemble) and the black dotted lines the 33 and 67 % quantiles for the baseline experiment.

lation of reflectance observations reduces the uncertainties in the estimation of the snowpack characteristics throughout the season. This is observed in Fig. 3, where the baseline experiment envelopes (blue shading) are narrower than those of the ensemble without assimilation (grey shading). In particular, the snow melt-out date is estimated much more accurately with the assimilation of reflectances: the uncertainty range drops from 24 days without assimilation to 9 days with assimilation.

Figure 4 shows the time evolution of the RMSE with assimilation at every observation time, at the end of the forecast step (blue solid line) and just after the filter analysis (blue dotted line). These results are compared to the RMSE without assimilation (red lines). The RMSE of the ensemble with assimilation is always lower than the RMSE without assimilation. Averaged over the season, a reduction of 46 % was obtained for SD and 44 % for SWE, (Table 2 – Baseline: seasonal RMSE for SD: 0.07 m; SWE: 19.7 kg m^{-2} compared to 0.13 m and 35.4 kg m^{-2} from the ensemble without assimilation). These results indicate the usefulness of using spectral optical radiance rather than albedo data since Dumont et al. (2012) obtained an improvement in SD estimate of only 14 % when assimilating albedo retrievals from MODIS sensor. It is remarkable that, despite the significant RMSE reduction in our experiment, there is most of the time no strong reduction of the RMSE from a single analysis. The reduced RMSEs with assimilation are consequently due to the successive observations throughout the season, highlighting the role of model dynamics.

The strongest RMSE reductions occur right after extended periods without precipitation and without available observations, when the reflectance ensemble spread is particularly pronounced (e.g., Fig. 3a). During these periods (e.g., from 7 to 14 December 2010, or from 11 to 21 January 2011), the ensemble uncertainties on reflectances, SD and SWE grow under the influence of the perturbed forcings including the perturbed impurity deposition rate. Observations of reflectances have a large impact when they are used. However, since reflectance observations are not very sensitive to the inner snowpack hidden by recent snowfalls, the uncertainties on SD and SWE accumulated earlier and not corrected by past analysis remain, which ultimately results in limited corrections on SD and SWE (Fig. 3, for example, on 28 January 2011), and sustained ensemble spreads and RMSE throughout the season.

After a significant snowfall, the uncertainties in SD and SWE may increase, and the assimilation of reflectances generally has a very small impact on these two variables. Indeed, the uncertainty in the amount of snowfall (translated here in perturbations on the snowfall rate) tends to increase the ensemble spread and RMSE on SD and SWE. Moreover, whether it be in the visible range of wavelengths sensitive to the impurity content or in the infrared part where changes on the microstructure dominates, a snowfall resets

Table 2. SD and SWE seasonal averaged RMSE computed with respect to the synthetic truth for all experiments over the 2010/2011 season. Results reported in Fig. 5 are the RMSE computed over the five selected seasons.

Results reported in variable assimilated assimilation timing	Fig. 1 No AD	Fig. 3 Refl. Baseline	Fig. S7[a] SD Clear sky days	Fig. S2[a] Refl. All days	Fig. S3[a] Refl. Accu.	Fig. S4[a] Refl. Melt	Fig. S5[a] Refl. Before Snowf	Fig. S6[a] Refl. After Snowf	Fig. S8[a] Refl. + SD	Fig. 5 Refl. All seasons
SD (m)	0.13	0.07	0.03	0.05	0.05	0.12	0.07	0.12	0.04	0.07
SWE ($kg\,m^{-2}$)	35.4	19.7	7.4	14.4	12.9	35.5	21.8	37.2	9.6	20.2

[a] See the Supplement.

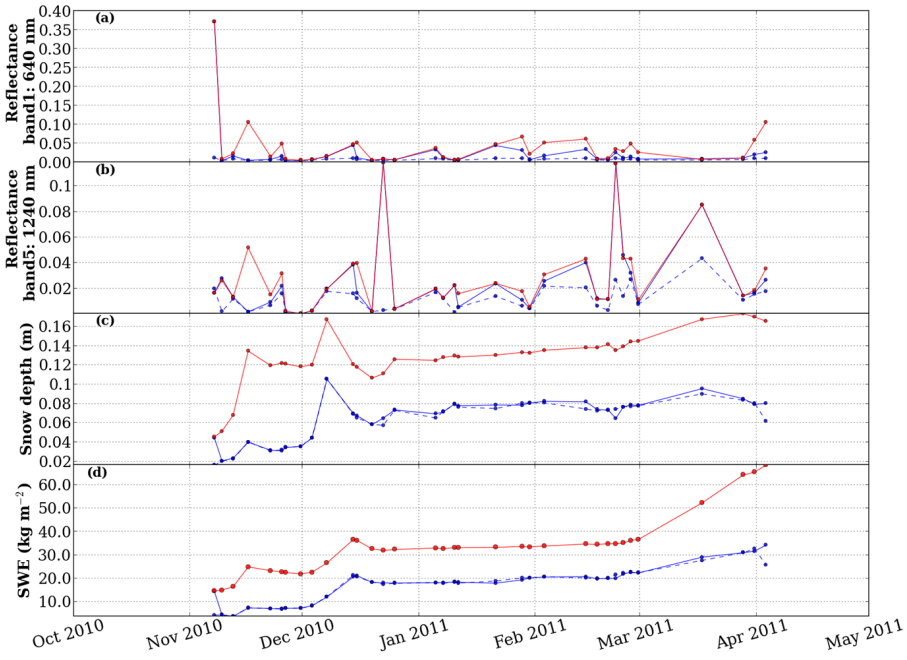


Figure 4. Time evolution of the ensemble RMSEs on **(a)** reflectance at 640 nm, **(b)** reflectance at 1240 nm, **(c)** SD and **(d)** SWE, over the 2010/2011 season, for the run without assimilation (red lines), and the baseline assimilation experiment (blue solid line: forecast; blue dotted line: analysis). Dots indicate analysis steps.

all ensemble members to the same set of reflectance values. This makes the discrimination between members using reflectances alone impossible, and the subsequent analysis provides a rather small uncertainty reduction for SD and SWE. This is illustrated on Fig. 3 on 10 November and on 1 December 2010, for example.

The remarks stated above for the season 2010/2011 hold for the other seasons. Figure 5 reports the time evolution of the SD and SWE RMSEs for all the selected seasons, in the experiments without assimilation (red lines) and with assimilation of reflectances (blue line; the experiments shown in green and black are discussed in the next section). On average, SD and SWE RMSEs are reduced by 45 and 48 %, respectively. This is comparable with results of Che et al. (2014), who assimilate radiances in the microwave spectrum from AMSR-E, and reduce the SD RMSE by 50 %. However, passive microwave observations are very sensitive to liquid water. Consequently, the performance of the assimilation during the melting period is reduced (Che et al. (2014) reduce the SD RMSE up to 61 % from January to March, during only the dry snow period). In contrast, our results show a well-marked reduction of errors near the end of the seasons (Fig. 4, red lines and blue dotted lines). Our results are also consistent with those from Liu et al. (2013) assimilating MODIS-derived snow cover fractions (SCFs), after a processing of the retrieval to improve accuracy of cloud coverage and snow mapping. Without this processing, the performance of SCF assimilation falls, with a SWE RMSE reduction near 10–20 %, similarly to Andreadis and Lettenmaier (2006).

Consequently, our ability to control the seasonal evolution of the snowpack with the assimilation of reflectances is demonstrated, though it exhibits limitations. In particular, the reduction of the snowpack SD and SWE ensemble spread greatly depends on the timing of the assimilated observations.

6 Sensitivity to the nature and the timing of observations

6.1 Impact of cloud coverage on the experiment

The presence of cloud coverage strongly reduces the number of optical data available for assimilation. To investigate impact of limiting the number of available observations, an experiment similar to the baseline experiment (see Sect. 5) is carried out, but assimilation is performed every day, (134 days) instead of 34 days in the baseline experiment. Figure S2 presents the results with the blue shading representing the envelopes of the ensemble assimilating daily MODIS-like observations and the grey shading representing the envelopes of the baseline experiment, reported from Fig. 3.

Obviously, in this second experiment, concerning the 640 nm reflectance variable, the spread of the ensemble is greatly reduced, efficiently fitting the observations (red dots) and its envelope does not show any extended periods with a large range of reflectance values anymore (Fig. S2a). Compared to the baseline experiment (grey envelopes), the uncertainty in the snow melt-out date is also reduced to 3 days. However during the major part of the winter, the SD and SWE ensemble spreads (Fig. S2b–c: blue envelopes) are comparable to the spreads obtained in the baseline experiment (Fig. S2b–c: grey envelopes). This is also reflected in Table 2 – All days: The seasonal RMSEs on SD and SWE are 0.05 m and 14.4 $\mathrm{kg\,m^{-2}}$, respectively, against 0.07 m and 19.7 $\mathrm{kg\,m^{-2}}$ in the baseline experiment. This shows that assimilating a limited number data due to realistic cloud conditions is not necessarily harmful to the estimation of the snowpack state. Note that this conclusion holds here for bulk variables such as SD and SWE. The estimation of other physical properties of the snowpack will be addressed in a future work using real observations.

6.2 On the timing of observations

The baseline experiment suggests that the timing of observations may largely determine the quality of the assimilation process. To explore the role of the timing, four additional assimilation tests are designed for which MODIS-like reflectances are assimilated (i) only at the beginning of the season (before 31 December 2010, Fig. S3: Accu), (ii) only in the second part of the snow season (after 31 December 2010, Fig. S4: Melt), (iii) only after several day-long periods without precipitation (Fig. S5: Before Snowf) and (iv) only right after snowfall events (Fig. S6: After Snowf).

In case i (Accu), results show that even if the SD and SWE spreads are reduced during the assimilation period, the assimilation has almost no effect on the snow estimates during the snow melt period. The ensemble spread at the end of the season returns to almost the same value than the experiment without assimilation. The uncertainty of the snow melt-out date is reduced to only 22 days, compared to 24 days without assimilation. As for case ii (Melt), the spread reduction becomes quite discernible roughly 2 months after the first assimilation date and never reaches the range of the baseline experiment. The uncertainty of the snow melt-out date is however reduced to 11 days. This demonstrates that it is essential to assimilate reflectances over the entire season to compensate the fast growth of the snowpack ensemble in response to the uncertainties in the meteorological forcing.

In both cases iii (Before Snowf) and iv (After Snowf), reflectances are assimilated at only seven dates of the season. Case iii (Before Snowf) exhibits a more pronounced SD and SWE spreads reduction compared to case iv (After Snowf). The uncertainty on the snow melt-out date drops to 9 days in case iii (Before Snowf), while it stays at 23 days in case iv (After Snowf). In absence of precipitation, the snow surface is aging, leading to a decrease of reflectance values and a spread of the reflectance ensemble (Fig. S5a). Therefore, an observation after such a period provides a significant amount of information and produces an efficient analysis. On the contrary, solid precipitation resets the reflectance to high values and limits the spread of the reflectance ensemble (Fig. S6a) leading to a limited efficiency of the ensemble analysis. Assimilating only a few synthetic observations well distributed in time nearly leads to the same uncertainty of SD and SWE estimates as the baseline experiment assimilating 34 observations (Table 2 – Before Snowf: seasonal RMSE SD: 0.07 m; SWE: 21.8 $\mathrm{kg\,m^{-2}}$ compared to baseline experiment 0.07 m and 19.7 $\mathrm{kg\,m^{-2}}$, respectively).

Consequently, the time distribution of the observation turns out to be a key element in the expected success of the assimilation of reflectance observations. The end of an extended period without precipitation, when the surface snow layer is aging, is the best time to assimilate reflectances.

6.3 Assimilation of snow depths

To better evaluate the impact of the reflectance assimilation, we here compare the baseline experiment to an experiment assimilating synthetic SD observations keeping the same time distribution of the observations. Apart from the different nature of the observations, the assimilation setup is the same as the one described in Sect. 5 including the time frequency of observations. The results are displayed in Fig. S7.

The assimilation of synthetic SD observations greatly improves the estimates of SD and SWE (Fig. S7b–c). The spread reduction is much stronger than with the assimilation of reflectance observations (Table 2 – SD, Clear sky days: the seasonal RMSE on SD and SWE are 0.03 m and 7.4 $\mathrm{kg\,m^{-2}}$, respectively, against 0.07 m and 19.7 $\mathrm{kg\,m^{-2}}$ in the baseline experiment) and is maintained throughout the season. The uncertainty range on the snow melt-out date is decreased to 8 days compared to 9 assimilating MODIS-like reflectances and 24 days without assimilation for the 2010/2011 season.

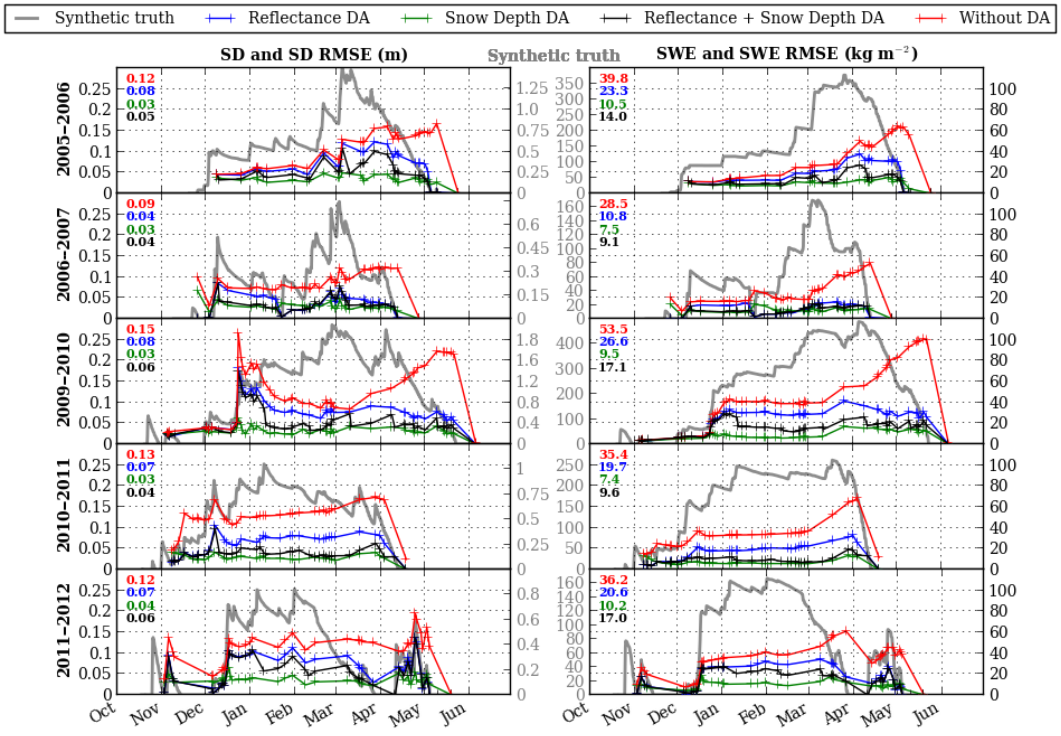


Figure 5. Time evolution of ensemble RMSEs on SD (left) and SWE (right) for the five seasons under study, for the run without assimilation (red lines), the baseline experiment (assimilating reflectances, blue lines), the experiment assimilating SD data (green lines) and the experiment assimilating combined reflectances and SD data (black lines). Crosses indicate analysis steps. Seasonal averages are displayed in the upper left corner of each graph. The model control simulation is represented by the grey lines, scaled by the "Synthetic truth" *y* axes.

Note that the spread reduction of the reflectance ensemble is very limited compared to the baseline experiment. This is consistent with the fact that while SD and SWE are better estimated in the case of SD simulation, the surface and inner physical properties of the snowpack are less impacted than in the case of assimilating reflectance observations.

Figure S7 shows that, at the beginning of the snow season (before 16 November 2010) and for a thin snowpack (less than 20 cm), SD assimilation seems to have less impact than reflectance assimilation. Indeed, with a thin snowpack, visible wavelengths penetrate down to the ground, and reflectance contains information on the whole snowpack. In this case, reflectance contains more information than SD. This could explain the better performance of the baseline experiment.

An additional experiment (not shown here) was also conducted assimilating daily synthetic SD observations because such measurements are usually available daily at about 60 different stations in the French Alps. This shows that, contrary to reflectance assimilation, for SD assimilation, the more frequent the observations, the greater the spread reduction (seasonal RMSE SD: 0.02 m; SWE: 4.7 kg m^{-2}).

Except for thin snow cover, the assimilation of SD observations outperforms reflectance assimilation in terms of SWE and SD estimates and seems to be less affected by the time distribution of the observations. When assimilating reflectance data, the ensemble needs to sufficiently spread (from an extended period without precipitation) to observe an impact of the assimilation (Fig. 3a). Inversely, and even if the reduction may be very small, every SD observations assimilation reduces the SD ensemble independently of the precipitation events (Fig. S7, excepted for thin snow cover).

Figure 5 also shows that, all these findings obtained for the 2010/2011 season are also verified for the five studied seasons. All assimilation experiments of synthetic SD observations reduce the RMSE with respect to both the model run without assimilation (red lines) and the experiments assimilation synthetic reflectances data (blue lines). However, in case of shallow snowpack, better performance is obtained using reflectance data.

6.4 Combining reflectance and snow depth assimilation

Though the assimilation of synthetic SD observations generally outperforms MODIS-like reflectance assimilation, spatially distributed SD measurements are rarely available over large areas on a daily basis. In situ SD observations give information only at the measurement point and many studies attest to the strong spatial variability of the snow cover (e.g., López-Moreno et al., 2011;

Veitinger et al., 2014; Bühler et al., 2015). Airborne lidar or ground-based laser lidar provide accurate SD measurements with fine resolution, but their low temporal frequency limits their utility for operational applications. So, one can imagine that over a mountain range, SD measurements are available at several locations for only a few dates in the season (e.g., occasional snow course, crowd-sourcing, ski resorts observations, ...). This scenario motivates the set-up of the following experiment. The experimental setup is the same as the baseline reflectance assimilation scheme previously described with an extra synthetic SD observation the 10th of each month. Results are shown in Fig. S8 and compared to the previous experiments in Fig. 5.

Combining the assimilation of MODIS-like reflectances with the assimilation of synthetic SD observations provides a benefit compared to assimilating reflectance only (Fig. 5, black and blue lines respectively). (i) In presence of a thin snow cover, the SD and SWE RMSEs of the combined reflectances and SD ensembles are reduced as the ones from the assimilation of the reflectance only. (ii) Almost all along the season, SD and SWE RMSEs remain below the reflectance assimilation RMSE thanks to SD assimilation. The combined assimilation leads to SWE seasonal RMSE of $9.6\,\mathrm{kg\,m^{-2}}$ to be compared to $7.4\,\mathrm{kg\,m^{-2}}$ for the experiment assimilating synthetic SD observations and $19.7\,\mathrm{kg\,m^{-2}}$ for the baseline reflectances assimilation experiment (Table 2).

These results indicate the usefulness of combining these two data sets in operational applications. Liu et al. (2013) reached a similar conclusion by combining the assimilation of SCF and SD (with a SWE RMSE reduction up to 72 %; up to 74 % in our study). However, given the strong spatial variability of the snow cover, the spatial representativity of punctual SD measurements may make their assimilation questionable. This issue should be addressed with experiments over two-dimensional, realistic domains.

7 Conclusions

This study investigates the assimilation of MODIS-like reflectances from visible to near-infrared (the first seven bands) into the multilayer snowpack model Crocus. The direct use of reflectance data instead of higher level snow products limits the introduction of uncertainties due to retrieval algorithms. For the assimilation, we implement a particle filter. A particle filter is chosen because (i) it is an ensemble method providing uncertainty estimates, and (ii) it is easily implemented (in comparison with other assimilation methods) with Crocus model, characterized by strong nonlinearities and its lagrangian representation of the snowpack layering. Given that the major source of error in snowpack simulations can be attributed to meteorological forcings, a stochastic perturbation method is designed to generate an ensemble of possible meteorological variables. This algorithm uses a first-order autoregressive model to account for the temporal correlations in the meteorological forcing uncertainties. This ensemble of meteorological forcings is then applied to generate the ensemble of snowpack simulations for the assimilation. Twin experiments are conducted at one point in the French Alps, the Col du Lautaret, over five hydrological years. The assimilated reflectance data corresponds to the first seven spectral bands of the MODIS sensors.

Reflectance assimilation using only data from clear-sky days reduces the SD and SWE seasonal RMSE by a factor close to 2. The uncertainty range on the snow melt-out date drops to 9 days compared to 24 without assimilation. Additional assimilation tests using different time distributions of the observations show that (i) reflectance assimilation greatly improves snowpack estimates if the observation comes after an extended period without precipitation, (ii) the assimilation has almost no impact if it comes right after a snowfall, and (iii) using only a few observations with the appropriate timing, i.e., after extended periods without precipitation, reduces RMSE almost as much as assimilating reflectances on a daily basis.

The assimilation of synthetic SD observations leads to a decrease of SD and SWE RMSE by a factor of more than 4. The uncertainty range on the snow melt-out date is reduced to 8 days. The assimilation of SD observations generally outperforms reflectance assimilation except for shallow snowpacks, typically less than 20 cm. However, whereas optical reflectance maps can be obtained daily thanks to spaceborne sensors such as MODIS or VIIRS, SD measurements are rarely available either over large areas or at the same time frequency. Combining reflectance assimilation with SD assimilation at four dates during the snow season leads to a decrease of SD and SWE RMSE by a factor close to 3.

This study provides a general theoretical framework to test the efficiency of several kinds of data assimilation in a snowpack model. This also highlights the benefit of using remotely sensed optical surface reflectance in the assimilation scheme to provide significant improvements of the snowpack SD and SWE estimates. Even if the assimilation of SD outperforms the assimilation using reflectance data, the sparsity of in situ measurements in space and/or time strongly reduces their utility in real data assimilation systems. Nevertheless, given their complementary features, combining remotely sensed reflectances and SD data, when available, would definitely improve snowpack simulations.

This study presents a first attempt to assimilate snow observations into the Crocus snowpack model with the overarching objective of improving operational snowpack forecasting. The next steps to proceed toward operational applications must include the assimilation of actual satellite data and the spatialization of the assimilation on larger domains. These steps include several challenges such as the increased calculation costs and degrees of freedom, and the need for a physically consistent 2-D meteorological ensemble, which will be addressed in future work.

Appendix A: Particle filter and sequential importance resampling, definitions (Gordon et al., 1993; Van Leeuwen, 2009, 2014)

In a discrete-time space model, the state of a system evolves according to

$$\boldsymbol{x}_k = f_k(\boldsymbol{x}_{k-1}, \boldsymbol{v}_{k-1}), \tag{A1}$$

where $\boldsymbol{x}_k$ is the state vector of the system at time k, $\boldsymbol{v}_{k-1}$ is the state noise vector and f_k is the non-linear and time-dependent function describing the evolution of the state vector.

Information about $\boldsymbol{x}_k$ is obtained through noisy measurements, $\boldsymbol{y}_k$, which are governed by the observation operator equation:

$$\boldsymbol{y}_k = h_k(\boldsymbol{x}_k, \boldsymbol{n}_k), \tag{A2}$$

where h_k is a possibly non-linear and time-dependent function linking the state vector to the observation (observation operator) and $\boldsymbol{n}_k$ is the measurement noise vector.

The filtering problem is to estimate sequentially the values of $\boldsymbol{x}_k$, given the observed values $y_0, \ldots, \boldsymbol{y}_k$, at any time step k. In a Bayesian setting, this problem can be formalized as the computation of the distribution $p(\boldsymbol{x}_k|\boldsymbol{y}_{1:k})$, which can be done recursively in the following two steps.

Prediction step:

$$p(\boldsymbol{x}_k|\boldsymbol{y}_{1:k-1}) = \int p(\boldsymbol{x}_{k-1}|y_{k-1})\, p(\boldsymbol{x}_k|\boldsymbol{x}_{k-1}) \mathrm{d}\boldsymbol{x}_{k-1}. \tag{A3}$$

Updating step to estimate $p(\boldsymbol{x}_k|\boldsymbol{y}_{1:k})$ using Bayes' rule:

$$p(\boldsymbol{x}_k|\boldsymbol{y}_{1:k}) \propto p(\boldsymbol{y}_k|\boldsymbol{x}_k)\, p(\boldsymbol{x}_k|\boldsymbol{y}_{1:k-1}). \tag{A4}$$

In the particle filter, the prior pdf is represented by equally weighted delta functions centered on the ensemble members or particles:

$$p(\boldsymbol{x}_{k-1}|\boldsymbol{y}_{1:k-1}) = \frac{1}{N}\sum_{i=1}^{N} \delta\left(\boldsymbol{x}_{k-1} - \boldsymbol{x}_{k-1}^i\right), \tag{A5}$$

where N is the ensemble size. With this representation, the propagation step Eq. (A3) provides

$$p(\boldsymbol{x}_k|\boldsymbol{y}_{1:k-1}) = \frac{1}{N}\sum_{i=1}^{N} \delta\left(\boldsymbol{x}_k - \boldsymbol{x}_k^i\right), \tag{A6}$$

where $\boldsymbol{x}_k^i = f(\boldsymbol{x}_{k-1}^i, \boldsymbol{v}_{k-1}^i)$; $\boldsymbol{v}_{k-1}^i$ is a realization of the noise $\boldsymbol{v}_{k-1}$. Then the analysis step follows with

$$p(\boldsymbol{x}_k|\boldsymbol{y}_{1:k}) = \sum_{i=1}^{N} w_k^i \delta\left(\boldsymbol{x}_k - \boldsymbol{x}_k^i\right), \tag{A7}$$

where the w_k^i are the particle weights, normalized to sum up to 1, and given by

$$w_k^i \propto p\left(\boldsymbol{y}_k|\boldsymbol{x}_k^i\right). \tag{A8}$$

To compute the weights, the error $\boldsymbol{n}_k$ of the observation operator h_k (Eq. A2) is often considered additive and Gaussian with mean 0 and covariance matrix R_k, so that the likelihood $p(\boldsymbol{y}_k|\boldsymbol{x}_k^i)$ writes

$$p(\boldsymbol{y}_k|\boldsymbol{x}_k^i) \propto \exp\left(-\frac{1}{2}\left(\boldsymbol{y}_k - h(\boldsymbol{x}_k^i)\right)^T R^{-1}\left(\boldsymbol{y}_k - h(\boldsymbol{x}_k^i)\right)\right). \tag{A9}$$

After the computation of the weights, the ensemble is resampled: particles with zero or negligible weights are ruled out; particles with large weights are duplicated a number of times commensurate with their weights. Several algorithms exist for this resampling step; we use the one of Kitagawa (Kitagawa, 1996).

The Supplement related to this article is available online at doi:10.5194/tc-10-1021-2016-supplement.

Acknowledgements. We wish to thank the two anonymous reviewers for their detailed comments. We gratefully acknowledge funding from Labex OSUG@2020 (Investissements d'avenir – ANR10 LABX56) and Fondation Eau Neige et Glace. This work has also been supported by the INSU/LEFE/MANU program. The development of the radiative model TARTES has been funded by the French ANR MONISNOW project, number ANR-11-JS56-0005.

Edited by: X. Fettweis

References

Abaza, M., Anctil, F., Fortin, V., and Turcotte, R.: Exploration of sequential streamflow assimilation in snow dominated watersheds, Adv. Water Resour., 80, 79–89, 2015.

Andreadis, K. M. and Lettenmaier, D. P.: Assimilating remotely sensed snow observations into a macroscale hydrology model, Adv. Water Resour., 29, 872–886, doi:10.1016/j.advwatres.2005.08.004, 2006.

Bartelt, P. and Lehning, M.: A physical SNOWPACK model for the Swiss avalanche warning: Part I: numerical model, Cold Reg. Sci. Technol., 35, 123–145, doi:10.1016/S0165-232X(02)00074-5, 2002.

Bavay, M., Grünewald, T., and Lehning, M.: Response of snow cover and runoff to climate change in high Alpine catchments of Eastern Switzerland, Adv. Water Resour., 55, 4–16, doi:10.1016/j.advwatres.2012.12.009, 2013.

Blayo, É., Bocquet, M., Cosme, E., and Cugliandolo, L. F.: Advanced Data Assimilation for Geosciences: Lecture Notes of the Les Houches School of Physics: Special Issue, June 2012, Oxford University Press, Oxford, UK, 2014.

Boone, A. and Etchevers, P.: An intercomparison of three snow schemes of varying complexity coupled to the same land surface model: Local-scale evaluation at an Alpine site, J. Hydrometeorol., 2, 374–394, doi:10.1175/1525-7541(2001)002<0374:AIOTSS>2.0.CO;2, 2001.

Brun, E., Martin, E., Simon, V., Gendre, C., and Coléou, C.: An energy and mass model of snow cover suitable for operational avalanche forecasting, J. Glaciol., 35, 333–342, 1989.

Brun, E., David, P., Sudul, M., and Brunot, G.: A numerical model to simulate snow-cover stratigraphy for operational avalanche forecasting, J. Glaciol., 38, 13–22, http://refhub.elsevier.com/S0165-232X(14)00138-4/rf0155, 1992.

Brun, F., Dumont, M., Wagnon, P., Berthier, E., Azam, M. F., Shea, J. M., Sirguey, P., Rabatel, A., and Ramanathan, Al.: Seasonal changes in surface albedo of Himalayan glaciers from MODIS data and links with the annual mass balance, The Cryosphere, 9, 341–355, doi:10.5194/tc-9-341-2015, 2015.

Bühler, Y., Marty, M., Egli, L., Veitinger, J., Jonas, T., Thee, P., and Ginzler, C.: Snow depth mapping in high-alpine catchments using digital photogrammetry, The Cryosphere, 9, 229–243, doi:10.5194/tc-9-229-2015, 2015.

Carmagnola, C. M., Morin, S., Lafaysse, M., Domine, F., Lesaffre, B., Lejeune, Y., Picard, G., and Arnaud, L.: Implementation and evaluation of prognostic representations of the optical diameter of snow in the SURFEX/ISBA-Crocus detailed snowpack model, The Cryosphere, 8, 417–437, doi:10.5194/tc-8-417-2014, 2014.

Carpenter, T. M. and Georgakakos, K. P.: Impacts of parametric and radar rainfall uncertainty on the ensemble streamflow simulations of a distributed hydrologic model, J. Hydrol., 298, 202–221, doi:10.1016/j.jhydrol.2004.03.036, 2004.

Castebrunet, H., Eckert, N., Giraud, G., Durand, Y., and Morin, S.: Projected changes of snow conditions and avalanche activity in a warming climate: the French Alps over the 2020–2050 and 2070–2100 periods, The Cryosphere, 8, 1673–1697, doi:10.5194/tc-8-1673-2014, 2014., 2014.

Che, T., Li, X., Jin, R., and Huang, C.: Assimilating passive microwave remote sensing data into a land surface model to improve the estimation of snow depth, Remote Sens. Environ., 143, 54–63, 2014.

Clark, M. P., Slater, A. G., Barrett, A. P., Hay, L. E., McCabe, G. J., Rajagopalan, B., and Leavesley, G. H.: Assimilation of snow covered area information into hydrologic and land-surface models, Adv. Water Res., 29, 1209–1221, 2006.

Cordisco, E., Prigent, C., and Aires, F.: Snow characterization at a global scale with passive microwave satellite observations, J. Geophys. Res.-Atmos. (1984–2012), 111, D19102, doi:10.1029/2005JD006773, 2006.

Dechant, C. and Moradkhani, H.: Radiance data assimilation for operational snow and streamflow forecasting, Adv. Water Resour., 34, 351–364, doi:10.1016/j.advwatres.2010.12.009, 2011.

De Lannoy, G. J. M., Reichle, R. H., Arsenault, K. R., Houser, P. R., Kumar, S., Verhoest, N. E. C., and Pauwels, V. R. N.: Multiscale assimilation of Advanced Microwave Scanning Radiometer–EOS snow water equivalent and Moderate Resolution Imaging Spectroradiometer snow cover fraction observations in northern Colorado, Water Resour. Res., 48, W01522, doi:10.1029/2011WR010588, 2012.

Deodatis, G. and Shinozuka, M.: Auto-regressive model for nonstationary stochastic processes, J. Eng. Mech.-ASCE, 114, 1995–2012, doi:10.1061/(ASCE)0733-9399(1988)114:11(1995), 1988.

Doherty, S. J., Grenfell, T. C., Forsström, S., Hegg, D. L., Brandt, R. E., and Warren, S. G.: Observed vertical redistribution of black carbon and other insoluble light-absorbing particles in melting snow, J. Geophys. Res.-Atmos., 118, 5553–5569, doi:10.1002/jgrd.50235, 2013.

Domine, F., Sparapani, R., Ianniello, A., and Beine, H. J.: The origin of sea salt in snow on Arctic sea ice and in coastal regions, Atmos. Chem. Phys., 4, 2259–2271, doi:10.5194/acp-4-2259-2004, 2004.

Dong, J., Walker, J. P., Houser, P. R., and Sun, C.: Scanning multichannel microwave radiometer snow water equivalent assimilation, J. Geophys. Res.-Atmos. (1984–2012), 112, D07108, doi:10.1029/2006JD007209, 2007.

Dumont, M., Durand, Y., Arnaud, Y., and Six, D.: Variational assimilation of albedo in a snowpack model and reconstruction of the spatial mass-balance distribution of an alpine glacier, J. Glaciol., 58, 151–164, doi:10.3189/2012JoG11J163, 2012.

Dumont, M., Brun, E., Picard, G., Michou, M., Libois, Q., Petit, J., Geyer, M., Morin, S., and Josse, B.: Contribution of light-

absorbing impurities in snow to Greenland/'s darkening since 2009, Nat. Geosci., 7, 509–512, doi:10.1038/ngeo2180, 2014.

Durand, M., Kim, E. J., and Margulis, S. A.: Radiance assimilation shows promise for snowpack characterization, Geophys. Res. Lett., 36, L02503, doi:10.1029/2008GL035214, 2009.

Durand, Y., Brun, E., Mérindol, L., Guyomarc'h, G., Lesaffre, B., and Martin, E.: A meteorological estimation of relevant parameters for snow models, Ann. Glaciol., 18, 65–71, http://www.igsoc.org/annals/18/igs_annals_vol18_year1993_pg65-71.html, 1993.

Durand, Y., Giraud, G., Brun, E., Mérindol, L., and Martin, E.: A computer-based system simulating snowpack structures as a tool for regional avalanche forecasting, J. Glaciol., 45, 469–484, 1999.

Essery, R., Morin, S., Lejeune, Y., and Menard, C. B.: A comparison of 1701 snow models using observations from an alpine site, Adv. Water Res., 55, 131–148, doi:10.1016/j.advwatres.2012.07.013, 2013.

Etchevers, P., Golaz, C., and Habets, F.: Simulation of the water budget and the river flows of the Rhone basin from 1981 to 1994, J. Hydrol., 244, 60–85, doi:10.1016/S0022-1694(01)00332-8, 2001.

Evensen, G.: Data assimilation: the ensemble Kalman filter, Springer Science and Business Media, Berlin, Germany, 2009.

Fortin, V., Abaza, M., Anctil, F., and Turcotte, R.: Why should ensemble spread match the RMSE of the ensemble mean, J. Hydrometeorol., 15, 1708–1713, doi:10.1175/JHM-D-14-0008.1, 2014.

Foster, J. L., Sun, C., Walker, J. P., Kelly, R., Chang, A., Dong, J., and Powell, H.: Quantifying the uncertainty in passive microwave snow water equivalent observations, Remote Sens. Environ., 94, 187–203, doi:10.1016/j.rse.2004.09.012, 2005.

Gabbi, J., Huss, M., Bauder, A., Cao, F., and Schwikowski, M.: The impact of Saharan dust and black carbon on albedo and long-term mass balance of an Alpine glacier, The Cryosphere, 9, 1385–1400, doi:10.5194/tc-9-1385-2015, 2015.

Gordon, N. J., Salmond, D. J., and Smith, A. F.: Novel approach to nonlinear/non-Gaussian Bayesian state estimation, IEE Proc.-F, 140, 107–113, 1993.

Hall, D. K. and Riggs, G. A.: Accuracy assessment of the MODIS snow products, Hydrol. Process., 21, 1534–1547, doi:10.1002/hyp.6715, 2007.

Jordan, R.: A One-Dimensional Temperature Model for a Snow Cover: Technical Documentation for SNTHERM. 89., Tech. rep., Cold Regions Research and Engineering Lab, Hanover, NH, USA, 1991.

Kitagawa, G.: Monte Carlo filter and smoother for non-Gaussian nonlinear state space models, J. Comput. Graph. Stat., 5, 1–25, 1996.

Lehning, M., Völksch, I., Gustafsson, D., Nguyen, T. A., Stähli, M., and Zappa, M.: ALPINE3D: a detailed model of mountain surface processes and its application to snow hydrology, Hydrol. Process., 20, 2111–2128, doi:10.1002/hyp.6204, 2006.

Li, W., Stamnes, K., Chen, B., and Xiong, X.: Snow grain size retrieved from near-infrared radiances at multiple wavelengths, Geophys. Res. Lett., 28, 1699–1702, doi:10.1029/2000GL011641, 2001.

Libois, Q., Picard, G., France, J. L., Arnaud, L., Dumont, M., Carmagnola, C. M., and King, M. D.: Influence of grain shape on light penetration in snow, The Cryosphere, 7, 1803–1818, doi:10.5194/tc-7-1803-2013, 2013.

Libois, Q., Picard, G., Dumont, M., Arnaud, L., Sergent, C., Pougatch, E., Sudul, M., and Vial, D.: Experimental determination of the absorption enhancement parameter of snow, J. Glaciol., 60, 714–724, doi:10.1002/2014JD022361, 2014.

Liu, Y., Peters-Lidard, C. D., Kumar, S., Foster, J. L., Shaw, M., Tian, Y., and Fall, G. M.: Assimilating satellite-based snow depth and snow cover products for improving snow predictions in Alaska, Adv. Water Res., 54, 208–227, doi:10.1016/j.advwatres.2013.02.005, 2013.

López-Moreno, J. I., Fassnacht, S. R., Beguería, S., and Latron, J. B. P.: Variability of snow depth at the plot scale: implications for mean depth estimation and sampling strategies, The Cryosphere, 5, 617–629, doi:10.5194/tc-5-617-2011, 2011.

Masson, V., Le Moigne, P., Martin, E., Faroux, S., Alias, A., Alkama, R., Belamari, S., Barbu, A., Boone, A., Bouyssel, F., Brousseau, P., Brun, E., Calvet, J.-C., Carrer, D., Decharme, B., Delire, C., Donier, S., Essaouini, K., Gibelin, A.-L., Giordani, H., Habets, F., Jidane, M., Kerdraon, G., Kourzeneva, E., Lafaysse, M., Lafont, S., Lebeaupin Brossier, C., Lemonsu, A., Mahfouf, J.-F., Marguinaud, P., Mokhtari, M., Morin, S., Pigeon, G., Salgado, R., Seity, Y., Taillefer, F., Tanguy, G., Tulet, P., Vincendon, B., Vionnet, V., and Voldoire, A.: The SURFEXv7.2 land and ocean surface platform for coupled or offline simulation of earth surface variables and fluxes, Geosci. Model Dev., 6, 929–960, doi:10.5194/gmd-6-929-2013, 2013.

Morin, S.: Observation and numerical modeling of snow on the ground: use of existing tools and contribution to ongoing developments, Habilitation à diriger des recherches, Université Joseph Fourier, Grenoble, France, available at: https://tel.archives-ouvertes.fr/tel-01098576 (last access: 12 May 2016), 2014.

Morin, S., Lejeune, Y., Lesaffre, B., Panel, J.-M., Poncet, D., David, P., and Sudul, M.: An 18-yr long (1993–2011) snow and meteorological dataset from a mid-altitude mountain site (Col de Porte, France, 1325 m alt.) for driving and evaluating snowpack models, Earth Syst. Sci. Data, 4, 13–21, doi:10.5194/essd-4-13-2012, 2012.

Navari, M., Margulis, S. A., Bateni, S. M., Tedesco, M., Alexander, P., and Fettweis, X.: Feasibility of improving a priori regional climate model estimates of Greenland ice sheet surface mass loss through assimilation of measured ice surface temperatures, The Cryosphere, 10, 103–120, doi:10.5194/tc-10-103-2016, 2016.

Noilhan, J. and Planton, S.: A simple parameterization of land surface processes for meteorological models, Mon. Weather Rev., 117, 536–549, doi:10.1175/1520-0493(1989)117<0536:ASPOLS>2.0.CO;2, 1989.

Painter, T. H., Barrett, A. P., Landry, C. C., Neff, J. C., Cassidy, M. P., Lawrence, C. R., McBride, K. E., and Farmer, G. L.: Impact of disturbed desert soils on duration of mountain snow cover, Geophys. Res. Lett., 34, L12502, doi:10.1029/2007GL030284, 2007.

Phan, X. V., Ferro-Famil, L., Gay, M., Durand, Y., Dumont, M., Morin, S., Allain, S., D'Urso, G., and Girard, A.: 1D-Var multilayer assimilation of X-band SAR data into a detailed snowpack model, The Cryosphere, 8, 1975–1987, doi:10.5194/tc-8-1975-2014, 2014.

Quintana Segui, P., Moigne, P. L., Durand, Y., Martin, E., Habets, F., Baillon, M., Canella, C., Franchisteguy, L., and Morel, S.: Analysis of near surface atmospheric variables: validation of the SAFRAN analysis over France, J. Appl. Meteorol. Clim., 47, 92–107, doi:10.1175/2007JAMC1636.1, 2008.

Raleigh, M. S., Lundquist, J. D., and Clark, M. P.: Exploring the impact of forcing error characteristics on physically based snow simulations within a global sensitivity analysis framework, Hydrol. Earth Syst. Sci., 19, 3153–3179, doi:10.5194/hess-19-3153-2015, 2015.

Reichle, R. H.: Data assimilation methods in the Earth sciences, Adv. Water Resour., 31, 1411–1418, 2008.

Sirguey, P., Mathieu, R., and Arnaud, Y.: Subpixel monitoring of the seasonal snow cover with MODIS at 250 m spatial resolution in the Southern Alps of New Zealand: methodology and accuracy assessment, Remote Sens. Environ., 113, 160–181, doi:10.1016/j.rse.2008.09.008, 2009.

Snyder, C., Bengtsson, T., Bickel, P., and Anderson, J.: Obstacles to high-dimensional particle filtering, Mon. Weather Rev., 136, 4629–4640, doi:10.1175/2008MWR2529.1, 2008.

Stankov, B., Cline, D., Weber, B., Gasiewski, A., and Wick, G.: High-resolution airborne polarimetric microwave imaging of snow cover during the NASA cold land processes experiment, IEEE T. Geosci. Remote S., 46, 3672–3693, doi:10.1109/TGRS.2008.2000625, 2008.

Sun, C., Walker, J. P., and Houser, P. R.: A methodology for snow data assimilation in a land surface model, J. Geophys. Res.-Atmos., 109, D08108, doi:10.1029/2003JD003765, 2004.

Tedesco, M., Reichle, R., Löw, A., Markus, T., and Foster, J. L.: Dynamic approaches for snow depth retrieval from spaceborne microwave brightness temperature, , IEEE T. Geosci. Remote S., 48, 1955–1967, doi:10.1109/TGRS.2009.2036910, 2010.

Van Leeuwen, P. J.: Particle filtering in geophysical systems, Mon. Weather Rev., 137, 4089–4114, doi:10.1175/2009MWR2835.1, 2009.

Van Leeuwen, P. J.: Particle filters for the geosciences, Advanced Data Assimilation for Geosciences: Lecture Notes of the Les Houches School of Physics: Special Issue, June 2012, p. 291, doi:10.1093/acprof:oso/9780198723844.003.0013, 2014.

Veitinger, J., Sovilla, B., and Purves, R. S.: Influence of snow depth distribution on surface roughness in alpine terrain: a multi-scale approach, The Cryosphere, 8, 547–569, doi:10.5194/tc-8-547-2014, 2014.

Vernay, M., Lafaysse, M., Mérindol, L., Giraud, G., and Morin, S.: Ensemble forecasting of snowpack conditions and avalanche hazard, Cold Reg. Sci. Technol., 120, 251–262, doi:10.1016/j.coldregions.2015.04.010, 2015.

Vionnet, V., Brun, E., Morin, S., Boone, A., Faroux, S., Le Moigne, P., Martin, E., and Willemet, J.-M.: The detailed snowpack scheme Crocus and its implementation in SURFEX v7.2, Geosci. Model Dev., 5, 773–791, doi:10.5194/gmd-5-773-2012, 2012.

Warren, S.: Optical properties of snow, Rev. Geophys., 20, 67–89, doi:10.1029/RG020i001p00067, 1982.

Warren, S. G. and Clarke, A. D.: Soot in the atmosphere and snow surface of Antarctica, J. Geophys. Res.-Atmos. (1984–2012), 95, 1811–1816, doi:10.1029/JD095iD02p01811, 1990.

Wright, P., Bergin, M., Dibb, J., Lefer, B., Domine, F., Carman, T., Carmagnola, C. M., Dumont, M., Courville, Z., Schaaf, C., and Wang, Z.: Comparing MODIS daily snow albedo to spectral albedo field measurements in Central Greenland, Remote Sens. Environ., 140, 118–129, doi:10.1016/j.rse.2013.08.044, 2014.